

Number 541



UNIVERSITY OF  
CAMBRIDGE

Computer Laboratory

## Different applications of two-dimensional potential fields for volume modeling

L. Barthe, N.A. Dodgson, M.A. Sabin,  
B. Wyvill, V. Gaildrat

August 2002

15 JJ Thomson Avenue  
Cambridge CB3 0FD  
United Kingdom  
phone +44 1223 763500  
<http://www.cl.cam.ac.uk/>

© 2002 L. Barthe, N.A. Dodgson, M.A. Sabin, B. Wyvill,  
V. Gaildrat

Technical reports published by the University of Cambridge  
Computer Laboratory are freely available via the Internet:

*<http://www.cl.cam.ac.uk/TechReports/>*

Series editor: Markus Kuhn

ISSN 1476-2986

# Different applications of two-dimensional potential fields for volume modeling

L. Barthe, N.A. Dodgson, M.A. Sabin, B. Wyvill and V. Gaildrat  
University of Cambridge, University of Cambridge,  
Numerical Geometry ltd, University of Calgary, University of Toulouse

August 29, 2002

## Abstract

Current methods for building models using implicit volume techniques present problems defining accurate and controllable blend shapes between implicit primitives. We present new methods to extend the freedom and controllability of implicit volume modeling. The main idea is to use a free-form curve to define the profile of the blend region between implicit primitives.

The use of a free-form implicit curve, controlled point-by-point in the Euclidean user space, allows us to group boolean composition operators with sharp transitions or smooth free-form transitions in a single modeling metaphor. This idea is generalized for the creation, sculpting and manipulation of volume objects, while providing the user with simplicity, controllability and freedom in volume modeling.

Bounded volume objects, known as “Soft objects” or “Metaballs”, have specific properties. We also present binary Boolean composition operators that gives more control on the form of the transition when these objects are blended.

To finish, we show how our free-form implicit curves can be used to build implicit sweep objects.

## 1 Introduction

Providing interactive, precise and intuitive control of shapes is a fundamental issue in the development of three dimensional modeling techniques. Direct manipulation of meshes, parametric shape representations and, more recently, sub-division surfaces are common and useful solutions adopted by most commercial software. Volume models are rapidly becoming a practical alternative to these methods due to the increase in computing power and storage capacity of modern workstations combined with the latest developments in graphics hardware. Better hardware along with improved volume visualization algorithms [1, 2] and data structures [3], allow us to interactively and accurately render iso-potential surfaces or potential variations in a volume.

A volume object is defined by a potential field  $f(p)$  that associates a potential value with each point  $p$  of the Euclidean space  $\mathbb{E}^3$ . Commonly used surface representations such as sub-division surface techniques do not provide a true three-dimensional representation of the object. A surface in a volume representation is a set of points defined with an iso-potential value (an implicit surface). Volume objects have several important advantages: inside and outside can be distinguished easily, they allow efficient collision tests, high quality triangle meshes of iso-potential surfaces [4], classical Boolean operations [5], blending [6, 7, 8], and more advanced sweeping by moving solid [9], Boolean composition with soft transitions [10, 11] and Constructive Volume Geometry algebra [12].

Most of these techniques are based on the blending properties of implicit surfaces. Early work used the addition operator between field values to provide smooth transitions (blends) between implicit primitives [6, 13, 14]. These transitions were approximately controlled by parameters embedded in the implicit function that defined these methods. Later work exploited the locality property of the primitives as a powerful method to build complicated objects from a small number of primitives combined with a large range of operators [11, 15]. Composition operators like the ones proposed by Hoffmann et al [16] and

Pasko et al [10] demonstrated that smooth transitions could be obtained using Boolean operators on volumes defined by the inequality  $f(p) \leq 0$  (see also [17]), and Barthe et al [18] showed that in a restricted application, accurate control of the transition could be obtained. One of the big advantages over other modelling techniques, is that a variety of composition operations can be easily performed between implicit primitives, thus accurate and intuitive control over these operations is a critical step to providing interactive and efficient volume modeling software.

The goal of this work is to provide methods that will simply and accurately control the transitions in composition operators and more generally increase the freedom in the manipulation of volume objects. We use the theoretical interpretation of composition operators described in [18]. This leads us from the definition of free-form implicit curves controlled point-by-point and with regular field variations, to the generalization of Boolean composition operators, sculpture and modeling tools in a unique operator based on the manipulation of this implicit free-form curve in the Euclidean modeling space. This greatly increases the simplicity, the controllability and the freedom in volume modeling. We also adapt one of our composition operators to provide union, intersection and difference Boolean operators with smooth transitions controlled point-by-point between implicit primitives (or *blobs*). In this paper, the term "blobs" refers to implicit primitives with local influence radius, also known as skeletal implicit primitives, "soft objects" or "metaballs". And finally, because we have defined free-form profiles with regular variations, we show how they can be swept to replace the single valued function used, until now, in implicit sweep objects. This allow us to extend the variety of shapes produced and to remove the limits brought by single valued profiles.

The organization of this paper is as follows: We first present a summary of the different modeling techniques commonly used to build volume objects. Bounded primitives (like "Soft Objects" [14]), real-functions and sampled potential field manipulations are described. It appears clear that, whatever the model used, improvements in control are desirable when volume primitives are composed.

This is followed by the presentation of free-form implicit curves and, more generally, their two-dimensional potential fields. Since these profiles are used to combine or define volumes, particular attention is focused on the variations of the field around the iso-potential curve. In this section, we present open and closed curves and we show the progress we have made in controlling the variations of the fields.

In Section 4 the application of free-form curves on volumes defined by the inequality  $f(p) \leq 0$  is presented. This category regroups and generalizes most of the volume primitives, as shown in [17]. The possibility of creating open or closed free-form curves allows us to merge the Boolean composition operators (with or without smooth transitions) and operators to sculpt or create primitives in a single modeling metaphor: the extrusion of the implicit curve  $G(X, Y) = 0$  in the "implicit space"  $\mathbb{I}^2$ . Whatever the operator, the user simply acts on the two combined potential functions  $f_1$  and  $f_2$  through the deformation of the implicit curve  $G(f_1, f_2) = 0$ . We briefly illustrate the interactive manipulation of the implicit curves in a two-dimensional section of the Euclidean modeling space using the modeling tool presented in [19] and we discuss the limits of the intuitiveness and accuracy of this process.

In Section 5, we explain why our free-form curves are not directly applicable to bounded implicit primitives and new Boolean composition operators with smooth transitions for blobs are defined. They have several desirable properties including  $C^1$  continuous potential fields with a bounded transition and a faithful reproduction of the field variations of the composed primitives. Operators for union, intersection and difference are defined. We obtain point-by-point control for deforming the transition with a function of  $\mathbb{R} \rightarrow \mathbb{R}$ , which does not give true free-form control of the transition. However, as we discuss, it is not obvious that, for blobs, this level of freedom is necessary at the transition level.

Free-form profiles can also be used in implicit sweep objects [20, 37]. Indeed only profiles defined by functions of  $R \rightarrow R$  are used in implicit modeling while there is no apparent reason to limit the user in the form of the profile he wants to sweep. In Section 6 we show how to replace usual sweep profiles defined by functions of  $R \rightarrow R$  by our free-form profiles to remove limitations on the profile form without adding any complexity for the user. The objects generated with our profiles have their field variations regular enough to be nicely blended with other volume objects.

## 2 Related Works

Two different categories of potential functions can be distinguished to model volume objects: The first form has functions which equal *zero* outside a boundary, and the second has functions which vary over the whole of space. This last form is more expensive in evaluation. Even though our paper only deals with non-bounded primitives, we briefly present both representation to allow the reader to clearly differentiate them.

“Metaballs” [13] or “Soft Objects” [14] are bounded objects defined by a potential function  $f$  equalling zero everywhere outside the object’s boundary. Inside this boundary, the potential varies from *zero* to *one* and the volume object is defined by the set of points of  $\mathbb{E}^3$  for which  $f(p) \geq C$  (where  $C$  is a pre-chosen value in  $]0, 1[$ ). A wide variety of primitives are available [7, 20], and the blend is automatically computed by summing the potential of the primitives. Many different blending functions [21, 22] and blending models [23, 24] have been proposed to control the smoothness of the transition region, but the operators remain limited to the blending and the control of which primitives must and must not blend. The locality of the definition and the capacity to be automatically blended allow modeling techniques based on these objects to be interactive [25, 26].

CSG composition operators are already supported by bounded primitives (using the Ricci’s *min/max* operators [5]) but  $C^1$  discontinuities are introduced in the potential field of the resulting object, altering the smoothness of the transition when it has to be blended, which is undesirable.

A solution using Ricci’s super-elliptic operator [5] to apply binary union and binary intersection operators with smooth transitions to implicit primitives has been proposed by Wyvill et al [11] (see Equation 1)

$$G(f_1, f_2) = (f_1^n + f_2^n)^{\frac{1}{n}} \quad (1)$$

The quality of the created objects [15] shows that complicated objects can already be built, but it also shows that further research is needed to increase the composition’s accuracy and variety to achieve better interactive control in the blend region.

On the other hand, R-functions (real functions) and sampled potential fields can be grouped into a second category [17] where potentials are given over all the Euclidean space  $\mathbb{E}^3$  and the volume object is defined by the inequality  $f(p) \leq 0$ . The opposite convention, where the volume is defined by  $f(p) \geq 0$ , can also be used. Bounded objects, described above, can be adapted to R-functions by considering only the distance field minus the radius of the primitive. Other primitives can be obtained from different sources when the potential field is reconstructed as a distance field [27, 28, 29]. These objects are fundamental for volume modeling, as much for the variety of primitives as for the generalization of volumes to a unified model. For R-function operators, volume objects are defined with the convention:  $f(p) \geq 0$ . It has been shown in [10] how to apply binary CSG operators (with or without smooth transitions), space mapping operators and others. Equation 2 gives the example of the union operator with smooth transitions.

$$G(f_1, f_2) = \left( f_1 + f_2 + \sqrt{f_1^2 + f_2^2} \right) + \frac{a_0}{1 + \left( \frac{f_1}{a_1} \right)^2 + \left( \frac{f_2}{a_2} \right)^2} \quad (2)$$

Parameters  $a_0, a_1, a_2$  control the form of the transitions that do not have boundaries. Many other operators have been proposed in the literature [16, 30, 8], but the level of control on the transition remains globally equivalent. To correctly blend primitives, operator  $G$  must satisfy specific properties that are well defined [8]. A binary operator  $G$  applied on potential functions  $f_1$  and  $f_2$  can be written as a two-dimensional potential function  $G(X, Y)$  composed with the combined three-dimensional potential functions  $f_1$  and  $f_2$  (Equation 3).

$$\begin{aligned} G : \mathbb{R}^3 &\rightarrow \mathbb{R} \\ (x, y, z) &\rightarrow pot = G(f_1(x, y, z), f_2(x, y, z)) \end{aligned} \quad (3)$$

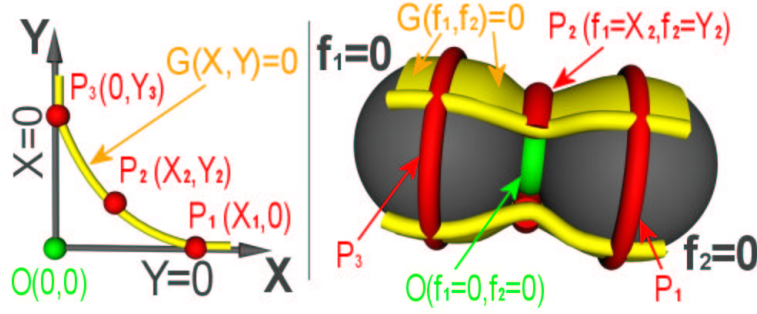


Figure 1: **Representation of the same profile  $G(X, Y) = 0$  in  $\mathbb{I}^2$  on the left and in  $\mathbb{E}^3$  on the right, when  $f_1$  and  $f_2$  are two spherical potential fields. The resulting iso-potential surface (in yellow on the right) has been cut away to show the details underneath.**

Barthe et al [18] introduced the notion of implicit extrusion fields. The function  $G$  is considered as a *zero* iso-potential curve  $G(X, Y) = 0$  defined in a two-dimensional “implicit space”  $\mathbb{I}^2$ . A two-dimensional “implicit space” can be seen as a curvilinear space in which each coordinate is a potential field (see Equation 4).

$$\begin{aligned} G : \mathbb{I}^2 &\rightarrow \mathbb{I} \\ (X, Y) &\rightarrow Z = G(X, Y) \\ \text{or } (f_1, f_2) &\rightarrow f_3 = G(f_1, f_2) \end{aligned}$$

$$\begin{aligned} \text{with } f_i : \mathbb{R}^3 &\rightarrow \mathbb{R} & i = 1..3 \\ (x, y, z) &\rightarrow \text{pot} = f_i(x, y, z) \end{aligned} \quad (4)$$

A point  $P(X = 3, Y = 2)$  (or  $P(f_1 = 3, f_2 = 2)$ ) in a space  $\mathbb{I}^2$  is then represented in the Euclidean space  $\mathbb{E}^3$  by the intersection between the 3 iso-potential surface of the field defined by  $f_1$  (which is the set of points  $p$  of  $\mathbb{E}^3$  for which  $f_1(p) = 3$ ) and the 2 iso-potential surface of the field defined by  $f_2$  (which is the set of points  $p$  of  $\mathbb{E}^3$  for which  $f_2(p) = 2$ ). This is the intersection between two surfaces which is generally a curve. A point  $P$  of  $\mathbb{I}^2$  is represented by a curve in  $\mathbb{E}^3$ . A curve (or profile) can be seen as a continuous succession of points. The profile of  $\mathbb{I}^2$  is then represented by a continuous succession of curves in  $\mathbb{E}^3$  (representing each point of the profile), which gives us the a surface. The profile  $G(X, Y) = 0$  defined in  $\mathbb{I}^2$  is said to be extruded in  $\mathbb{E}^3$  along the intersections of  $f_1$  and  $f_2$  iso-potential surfaces (Figure 1). The surface defined by the extrusion of profile  $G = 0$  is the result of combining  $f_1$  and  $f_2$ .

Full details are given in [18]. The authors explain how points and vectors defining the profile in  $\mathbb{I}^2$  can be directly selected by the user in Euclidean space  $\mathbb{E}^3$ , allowing accurate and intuitive control of the profile, and, therefore, of the resulting object. The profile  $G = 0$  is defined by a function  $H : \mathbb{R} \rightarrow \mathbb{R}$  such as  $Y = H(X)$  and  $G = Y - H(X)$ . This greatly limits the freedom given to the user, and moreover removes a part of the intuitive process. It also obliges the authors to propose specific operators for the union, intersection and difference with a “functionally-defined” transition, which is a smooth transition defined point-by-point from the Euclidean space  $\mathbb{E}^3$  with a single valued function  $H : \mathbb{R} \rightarrow \mathbb{R}$ . Functions  $H$  are defined with one-dimensional cubic polynomial splines [32] to interpolate the control points. Equation 5 shows the operator used for the union operator.

$$G(f_1, f_2) = \min(f_1, f_2) - H(|f_1 - f_2|) \quad (5)$$

This union operator (first proposed by Dekkers et al [31]) is built with a *min* function which requires the  $C^1$  continuity to be explicitly controlled where  $f_1 = f_2$ . Our conclusion is that this model represents a very interesting theoretical base and more research has to be done on profile definition to exploit the

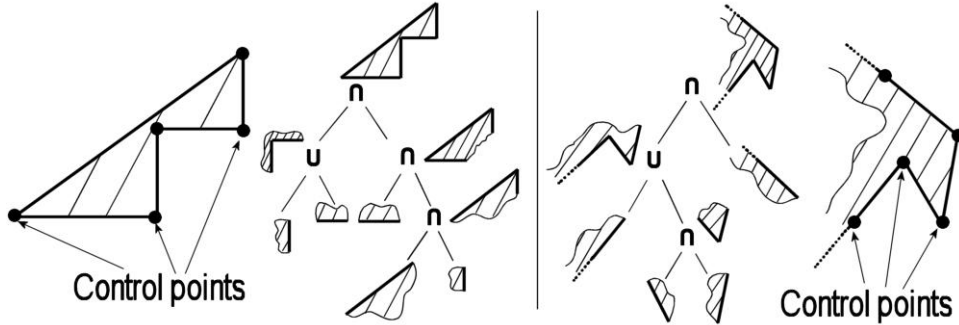


Figure 2: Example of binary composition trees to represent a polygon or an open curve by a real function.

properties of profile extrusion and point-by-point control from the Euclidean modeling space in a more powerful and intuitive volume modeling tool. To build a curve  $G(X, Y) = 0$  like the one shown in Figure 1, free-form implicit curves are needed (the vertical  $X = 0$  can not be defined with a single valued function). This leads us to the study of implicit free-form profiles controlled point-by-point.

### 3 Implicit Free-Form Curves

In this section we present our free-form implicit curves. We propose the use of homogenous control parameters to provide an intuitive solution to the user and for this reason we use free-form implicit curves controlled point-by-point as a means of providing accurate and intuitive operators on volumes. The composition of two primitives gives a new object which can be used as a primitive in a new composition. Because the smoothness and the control of the form of the transition is highly dependant on the variational properties of the primitives' fields, potential fields used to combine them must preserve these properties as faithfully as possible. This is why particular attention has to be focused on the regularity of the field variations produced by our two-dimensional potential fields  $G$ .

It appears natural to try to use methods like the implicitization of parametric free-form curves [33, 34] or the projection of the  $z$  value of a surface defined by an equation  $z = f(x, y)$  to define the implicit free-form curve. But these methods provide bounded functions while we need to be able to produce infinite open curves with the control of their limits. The first solution provides complicated equations and does not ensure regular and homogenous potential field variations, and the second requires the user to design the entire surface to create the profile and its variations, while they should be uniquely concentrating on the form of the curve. For these reasons we use a different approach.

As shown by Pasko et al [36], it is possible to represent polygons with straight and curved edges by real functions. The polygon is decomposed in a binary composition tree where the leaves are lines and the nodes are union or intersection R-function operators (see Figure 2). This method also avoids internal and unwanted zeroes. We choose it as a starting point to create our profiles. Indeed, it can easily be adapted to open profiles, and because lines are combined, the extremities are perfectly controlled: They are simply half lines. To provide a regular base for the field variations, we use lines defined by the zero iso-potential of a linear potential function  $l(X, Y)$ . The linear potential function  $l$  splits the space into two half spaces: One where  $l(X, Y) < 0$  (inside) and one where  $l(X, Y) > 0$  (outside). Function  $l$  has the one iso-potential line at a distance of one from the zero iso-potential (the one iso-potential line is in the outside half space defined by  $l$ , and the minus one iso-potential line in the inside half space). Because control points are used, line equations are defined with pairs of points. Even if R-function Boolean composition operators without smooth transition [10] already provide a potential field that is  $C^1$  continuous when both arguments are not equal to zero (they are both equal to zero at the junction between two zero iso-potential lines), they have a global impact on the line potential fields. This is a fundamental property because the variation of the combined primitives directly depends on the variation of the field of the composition operator and we want to provide volume objects with regular and smooth  $C^1$  continuous potential fields.

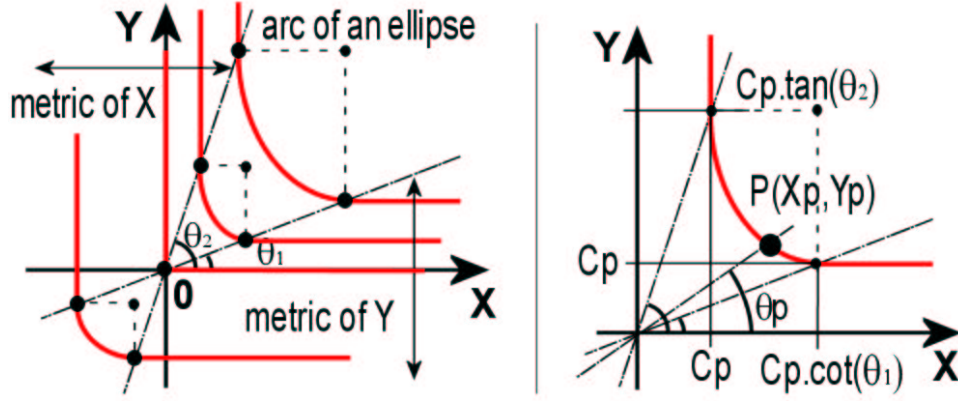


Figure 3: In red, on the left, representation of the two-dimensional field iso-potential curves defining our  $C^1$  continuous union operator  $\widehat{g}_\cup(X, Y)$ . On the right, graph of the  $C_P$  iso-potential curve and important values for computing the equation of the arc of an ellipse.

To ensure more faithful conservation of the field variations, we propose a new operator that modifies line potentials only around their junction. Indeed, the line metric reproduces the metric of  $X$  and  $Y$  (as shown in Figure 3), i.e. the metric the potential functions  $f_1$  and  $f_2$  once used as a composition operator. For convenience, we propose the following terminology:  $\widehat{g}_\cup, \widehat{g}_\cap, \widehat{g}_\setminus$  represent respectively our  $C^1$  continuous Boolean union, intersection and difference operators. Operator  $\widehat{g}_\cup(X, Y)$  (see Figure 3 and Equation 6) is defined by the fields of which it is composed outside a region bounded by two angles  $\theta_1$  and  $\theta_2$ , and by an arc of an ellipse inside it. If the angles are close to one another, the field is sharp at the transition level and if  $\theta_1$  is close to *zero* and  $\theta_2$  close to  $\pi/2$ , the field is highly smoothed. We suggest the use of  $\theta_1 = \pi/8$  and  $\theta_2 = 3\pi/8$ , which gives a good average between a smooth field and the conservation of  $X$  and  $Y$  metrics.

$$\theta_1 \in ]0, \pi/4[, \quad \theta_2 \in ]\pi/4, \pi/2[.$$

$$\text{At a point } P(X_P, Y_P) : \quad \theta_P = \text{angle}([OX], [OP])$$

$$\text{if } X_P = Y_P = 0 \quad \widehat{g}_\cup(X_P, Y_P) = 0$$

$$\text{if } \theta_P \in [\theta_2 - \pi, \theta_1] \quad \widehat{g}_\cup(X_P, Y_P) = Y_P$$

$$\text{if } \theta_P \in [\theta_2, \theta_1 + \pi] \quad \widehat{g}_\cup(X_P, Y_P) = X_P$$

$$\text{if } \theta_P \in ]\theta_1, \theta_2[ \quad \widehat{g}_\cup(X_P, Y_P) = C_P$$

where  $C_P$  is the solution of :

$$\frac{(C_P \cdot \cot(\theta_1) - X_P)^2}{(C_P \cdot \cot(\theta_1) - C_P)^2} + \frac{(C_P \cdot \tan(\theta_2) - Y_P)^2}{(C_P \cdot \tan(\theta_2) - C_P)^2} = 1$$

$$\text{if } \theta_P \in ]\theta_1 + \pi, \theta_2 + \pi[ \quad \widehat{g}_\cup(X_P, Y_P) = C_P$$

where  $C_P$  is the solution of :

$$\frac{(X_P - C_P \cdot \cot(\theta_2))^2}{(C_P - C_P \cdot \cot(\theta_2))^2} + \frac{(Y_P - C_P \cdot \tan(\theta_1))^2}{(C_P - C_P \cdot \tan(\theta_1))^2} = 1 \quad (6)$$

Equation 6 appears, at first glance, to be difficult to solve, but it can be greatly optimized, and most of the terms can be pre-computed. The closed form solution for the evaluation of  $C_P$  is given in Appendix C. Operators  $\widehat{g}_\cap$  and  $\widehat{g}_\setminus$  are built following the same construction and the same kind of equations are produced (their equations are given in Appendix A). With these operators, or with R-functions, free-form profiles  $G$  can be created. They are not smooth curves, but a succession of line segments, beginning and ending

	<i>min max</i>	R-functions	$\widehat{g}$	Barthe et al
open	106	148	457	135
closed	178	254	802	227

Table 1: Time in milliseconds to compute potential function values for the pictures shown in Figure 4. Picture size is  $512^2$  pixels, which corresponds to 262144 evaluations. The open curves are built with six line segments and the closed curves are built with ten segments.

with a half line if they are open. To obtain smooth curves, we use the Boolean operators proposed in [18]. These operators provide a point-by-point control of a “functionally-defined” transition and, because they are defined from functions of  $\mathbb{R} \rightarrow \mathbb{R}$ , they provide regular and smooth field variations. The first point, the middle point and the last point of the transition are then accurately controlled, which allows us to replace the sharp transition by a simple smooth transition automatically joining the middle of each segment. An exception is made for open curves where the beginning half-line is composed from the first control point and the last one is composed to the last point. The middle point is used to select the smoothness of the transition if necessary, but we recommend fixing it at a constant value to generate a smooth transition automatically and avoid the manipulation of an additional parameter.

Figure 4 shows the difference of field variations obtained using different composition operators in both an open and a closed profile  $G$ . Ricci’s *min* and *max* Boolean composition operators [5] leave the metric of the combined primitives unchanged (Figure 4(a)). This is why the potential field computed with the evaluation of the composition tree defining the profile  $G$  with these operators gives a valid reference to evaluate the variations of the metric once the operators applied to compute the profile. Figure 4(b) shows how potential fields obtained using Pasko’s R-function operators [10] are degraded in some areas (bottom left corner for the open profile figure and bottom for the closed profile figure). As we see, our operators  $\widehat{g}_{\cup}$  and  $\widehat{g}_{\cap}$  consequently increase the fidelity of the field variation for “segment profiles” (Figure 4(c)), and Barthe et al operators allow us to produce a smooth free-form implicit curve with regular and quite homogenous variations in its potential field (Figure 4(d)). For these reasons, our profiles satisfy the essential properties to define combination operators on volume objects in efficient and controllable modeling tools. Computing times are given in Table 1 to compare the cost of the different operators used to create free-form profiles. We can note that the use of our new operators  $\widehat{g}$  will increase the evaluation time of the curve by an average factor  $\simeq 3.1$ , while smooth curves are more time efficient than the sharp ones produced with the R-function composition operators.

## 4 Extrusion of Free-Form curves

We now present the application of our operators, based on a general representation of volumes. A volume object is defined by the inequality  $f(p) \leq 0$ . In this representation, function  $f$  does not uniformly return a fixed scalar (*zero* for blobs) outside a fixed boundary. This gives more freedom to produce new operators and to manipulate volumes. As we explained in Section 2, this representation allows the integration of a wide variety of different volume primitives [17]. However composition operators remain controlled by parameters embedded in an equation without an explicit link with a geometric parameter manipulable by the user in a graphic interface. Barthe et al [18] give a solution to introduce point-by-point control of the transition, and limitations of their method are discussed in Section 2. In this section we show how our free-form profiles  $G$  allow us to exploit the interpretation of “implicit space” to greatly increase freedom, accuracy and intuitive modeling in the manipulation of volumes. In fact, our method allows us to combine composition, sculpting and modeling tools in a single operator.

Following Barthe et al [18], a two-dimensional function  $G(X, Y)$  can be defined in an “implicit space”  $\mathbb{I}^2$  to generate a volume object. The “implicit space” is defined by two potential functions of  $\mathbb{R}^3 \rightarrow \mathbb{R}$ ,  $f_1$  and  $f_2$ . As shown in Figure 1 and explained in Section 2, the profile is said to be extruded along the intersections of  $f_1$  and  $f_2$  iso-potential surfaces. In fact, the choice of potential functions  $f_1$  and  $f_2$  define the trajectories of extrusion while the profile defines the free-form implicit curve which is going to be extruded along these trajectories (Figure 5).

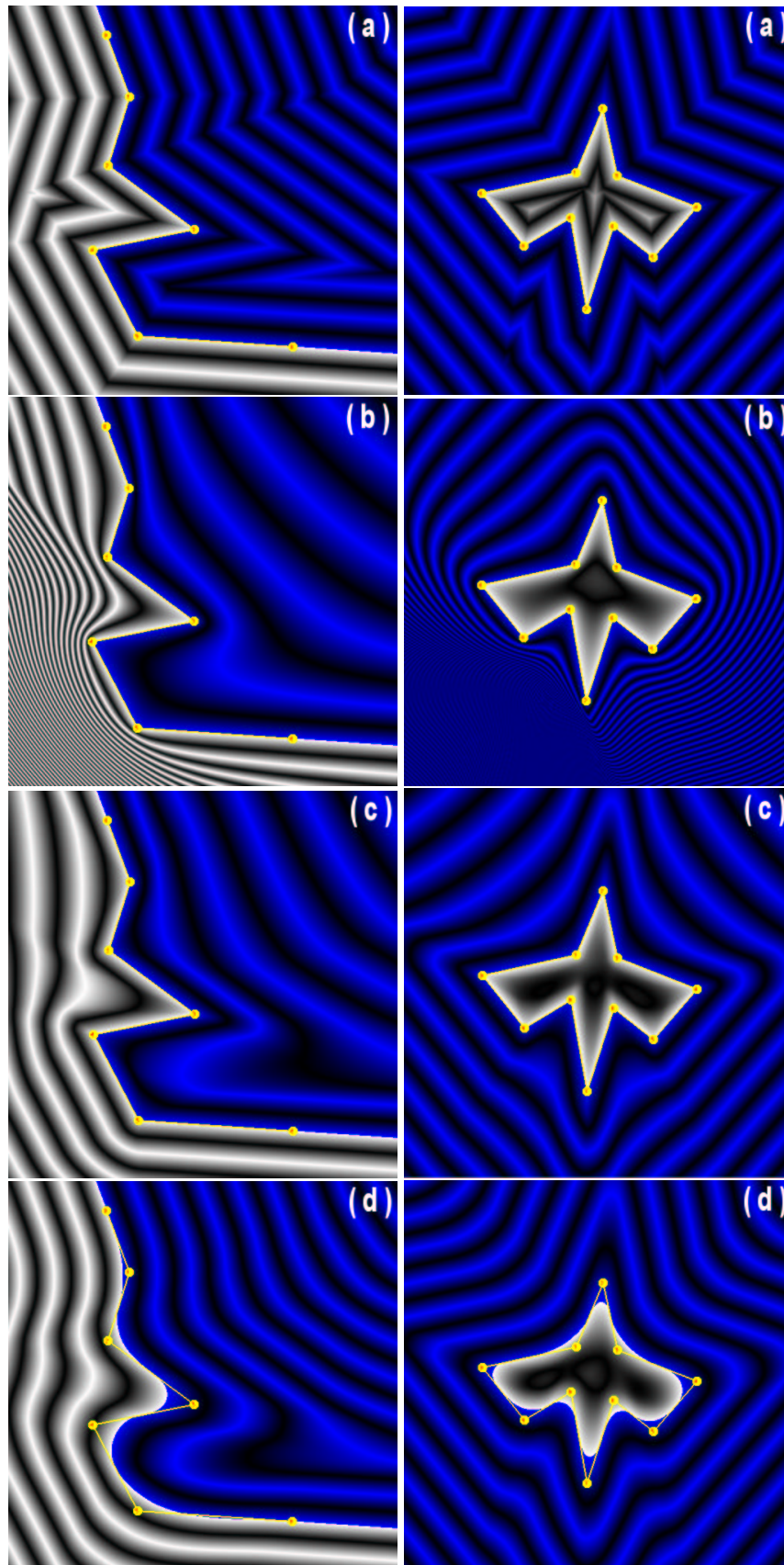


Figure 4: Open and closed implicit free-form two-dimensional potential fields  $G$  built with different operators: (a) Ricci's  $\min$  and  $\max$  operators, (b) R-functions, (c)  $\hat{g}_U$  and  $\hat{g}_r$ , and (d) Barthe et al operators with smooth transitions. The white contours correspond to  $G \leq 0$  and the blue ones to  $G > 0$ . The control points and the corresponding lines are drawn in yellow.

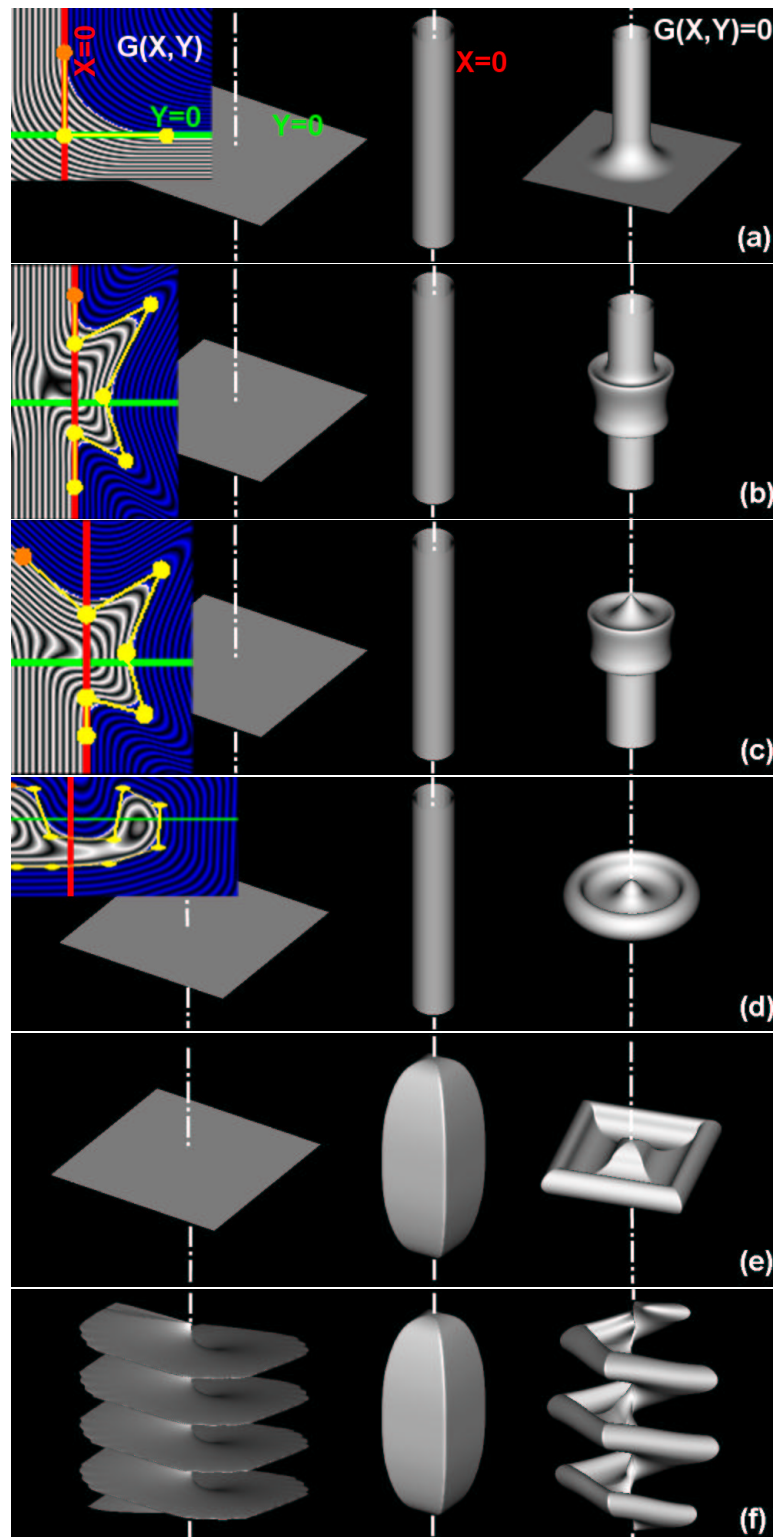


Figure 5: Figures (a) to (d) show different profiles extruded in an implicit field  $\mathbb{I}^2$  defined by a cylindrical potential field (for the abscissa  $X \equiv f_1$ , in the central column) and a plane field (for the ordinate  $Y \equiv f_2$ , in the left column). Profiles are shown in the top left corner. They are extruded around the cylinder, following the horizontal direction given by the plane. The final object produced by the extrusion of the profile is shown in the right column. In Figures (e) and (f), the profile is the one used in Figure (d). Figure (e) illustrates the modification in the extrusion when the cylinder is replaced by a closed parallelepiped object, and Figure (f) illustrates the modification obtained when the plane is replaced by a screw-like object. The result in (f) is that the profile is extruded around the parallelepiped, following the iso-surfaces of the screw.

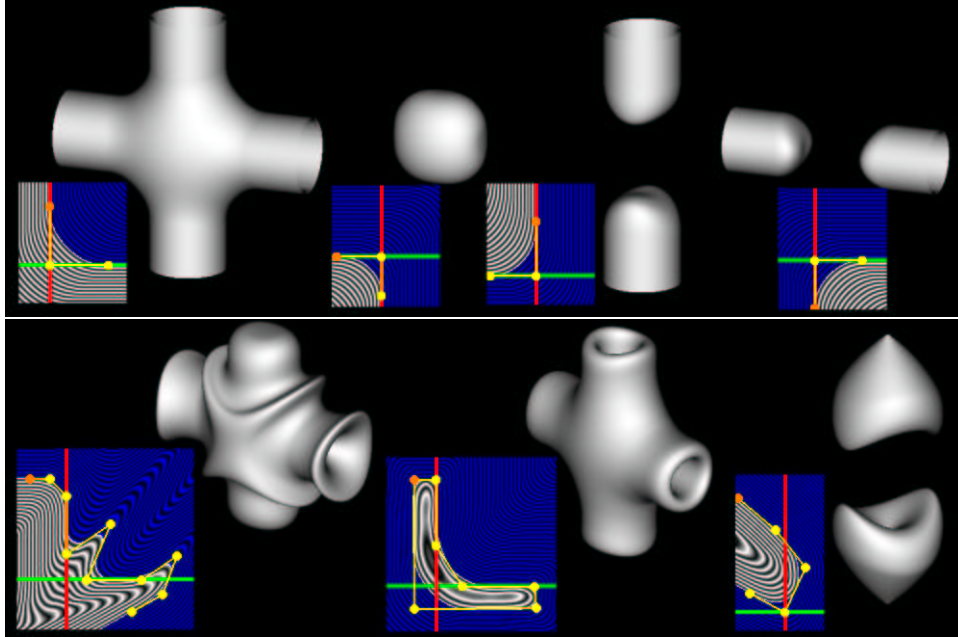


Figure 6: Different free-form profile extrusions in a “implicit space” defined by two orthogonal cylinders. The top row shows classical union, intersection and the two difference operators with smooth transitions. The following row illustrates more advanced possibilities offered by our free-form profile extrusion. In the profile pictures, the red line represents  $X = 0$  and the green line  $Y = 0$ .

The properties that a profile  $G$  must respect in order to provide the union Boolean composition operator with smooth transitions are well known [8], and “extrusion” properties of the profile are discussed in [18]. We simply recall bases to allow the reader to understand the “extrusion” mechanism. When the profile follows the  $X$  axis (which corresponds to the line  $Y = 0$ ), its representation in  $\mathbb{E}^3$  follows the *zero* iso-potential surface of the field defined by  $f_2$  and when it follows the  $Y$  axis (which corresponds to the line  $X = 0$ ), its representation in  $\mathbb{E}^3$  follows the *zero* iso-potential surface of the field defined by  $f_1$  (see Figure 1). These properties allow us to integrate the *zero* iso-potential surfaces of primitives defined by  $f_1$  and  $f_2$ , and to realize the Boolean composition operators with smooth transitions. Furthermore, as shown in Figure 6, more than classical smooth transitions, the profile can be used to sculpt the primitives and to combine them with free-form transitions.

The link between the profile and the shape of the resulting object becomes less intuitive when profiles are complicated. However, profile control points can be directly selected from the Euclidean space  $\mathbb{E}^3$ . Our volume objects are built and visualized using the modeling method proposed in [19]. We briefly summarized this approach to illustrate the controllability of our operators. Volumes are stored in a regular grid and visualized with a raycasting rendering using a triquadratic reconstruction [38]. A plane section of the potential values is extracted from the grid and visualized as a picture in a new window (Figure 7 (a) and (b)). In this window, the user can interactively select the profile without the abstraction of the form of the iso-potential surfaces of potential fields  $f_1$  and  $f_2$  (Figure 7 (c) and (d)). This shows that being able to select the control points, and thus the profile directly in the Euclidean space  $\mathbb{E}^3$ , restores the accuracy lost by the definition of the profile in an “implicit space”. Moreover, to exactly follow the *zero* iso-potential surface of potential function  $f_1$  or  $f_2$ , the abscissa or the ordinate of a profile control points can be explicitly fixed to *zero*. This is important when profiles are used to combine primitives.

With our approach, a wide variety of shapes and transitions can be produced, including all the ones that Barthe et al’s models [18] could generate (because free-form profiles generalize “functionally defined” ones). Furthermore, instead of disparate notions of composition operators, sculpture operator or primitive creation tool, we present a unified modeling metaphor which is simply: Choose the adequate potential functions

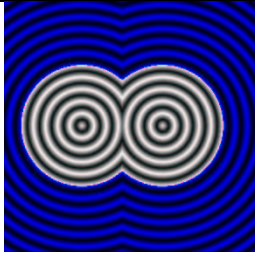
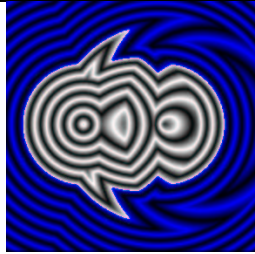
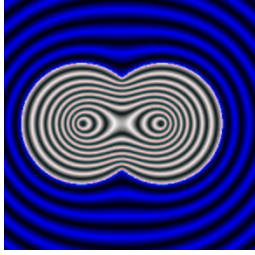
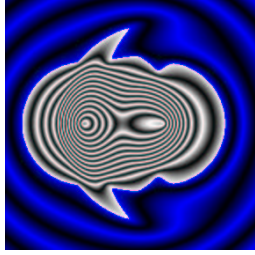
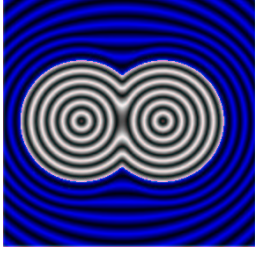
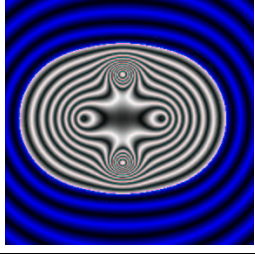
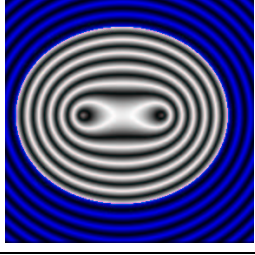
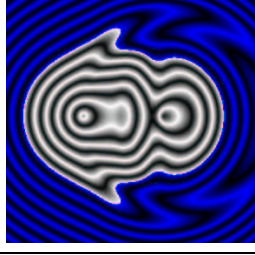
time	2D section	time	2D section
263		1025	
326		1448	
1057		5238	
369		not used	
322		1363	

Table 2: Time in milliseconds to compute potential function values for a  $128^3$  grid (2097152 evaluations). In the first column: (1<sup>st</sup> row) the Ricci's *min max* operators, (2<sup>nd</sup> row) the sharp R-functions operators, (3<sup>rd</sup> row) our operators  $\hat{g}$ , (4<sup>th</sup> row) the blending R-functions operators and (5<sup>th</sup> row) our free-form curve operator. Time and potential field variations (in a two-dimensional plane section) are shown : On the left for the classical sharp/blending operators and on the right, for a free-form operator created with seven segments.

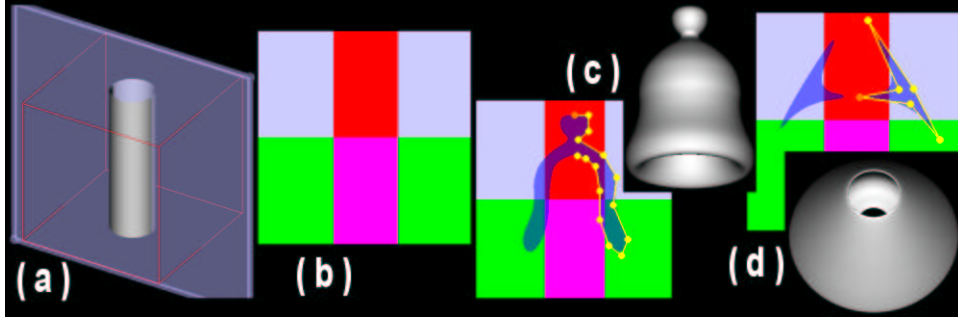


Figure 7: (a) Three dimensional visualization of volume objects and selection of the plane section in transparent blue. (b) Visualization of the plane section. Functions  $f_1$  and  $f_2$  are respectively: a vertical cylinder and an horizontal plane. Colors are used to easily identify different regions: red if  $f_1 \leq 0$  and  $f_2 \geq 0$ , green if  $f_1 \geq 0$  and  $f_2 \leq 0$ , purple if  $f_1 < 0$  and  $f_2 < 0$ , bright gray if  $f_1 > 0$  and  $f_2 > 0$ . (c) The section of the resulting object is visualized in blue with a transparency effect. We show an example of an open profile and its result. (d) Another example with a closed profile and its result.

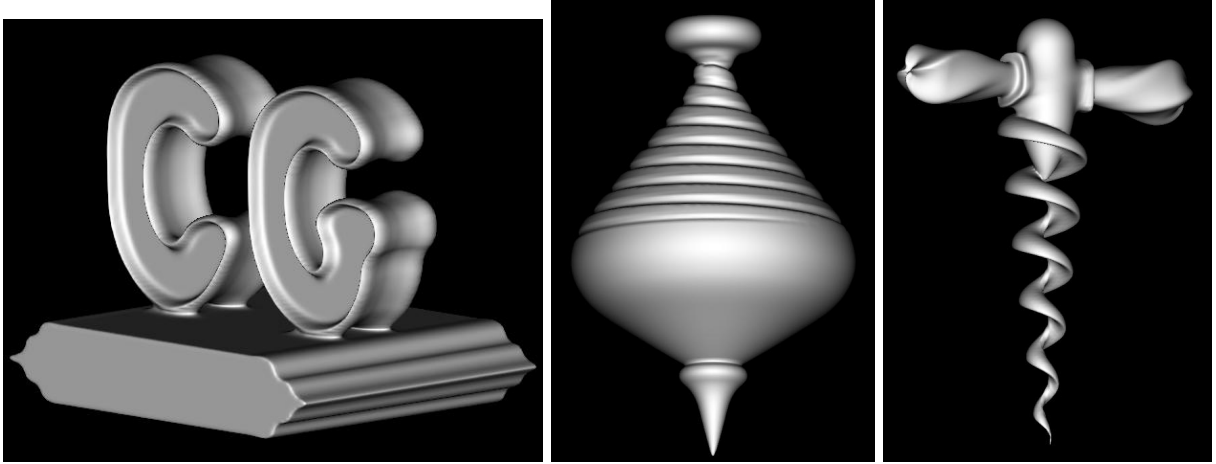


Figure 8: Examples of volume objects illustrating composition, sculpting and primitive creation using operators based on two-dimensional free-form potential fields.

$f_1$  and  $f_2$  and create the profile  $G$  to generate the new object. Once this process is well understood, our method is intuitive, and it provides a lot of freedom for the user to build different “implicit spaces” and extrude profiles in them (Figure 8). In addition, profiles can be directly defined and manipulated from the user modeling space  $\mathbb{E}^3$ . This makes our model relevant for interactive volume modeling. The limitations are essentially the complexity of the shape and the irregularity of the variations in the potential fields function  $f_1$  and  $f_2$ . Table 2 illustrates the simple example of the composition of two spheres, the differences of computing time and the variations in the object potential field.

## 5 Boolean Composition Operators with Smooth Transition for Blobs

We now focus on a bounded representation of volumes. We explain why we do not use our free-form profiles but rather the operators  $\widehat{g}_U$  and  $\widehat{g}_\cap$ . We show how they can be adapted to greatly increase the control and the regularity of the variation of the union and difference operators with smooth transitions on blobs. We also present a solution to produce a difference operator with the same essential properties.

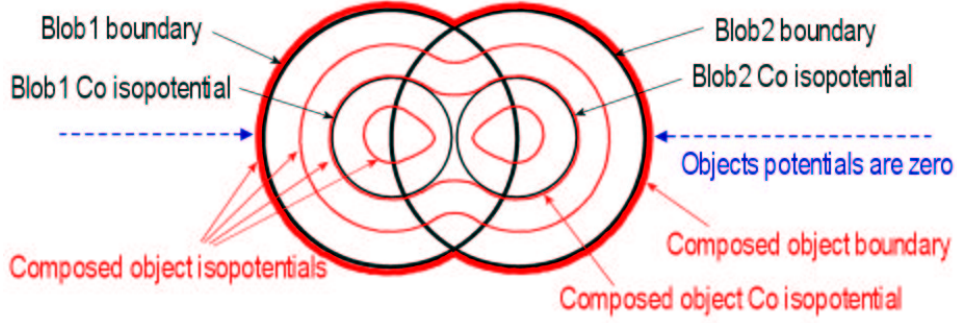


Figure 9: Representation of the field of an adequate union operator to compose two spherical blobs with a smooth transition.

A Blob is defined by the  $C_0$  iso-potential surface of its potential field  $f$ . The potential function  $f$  is bounded and varies as an approximation of a Gaussian from *one* at its “center” to *zero* on its boundary. Outside its boundary, the function  $f$  uniformly equals *zero*. At least four essential properties have to be taken into account to propose adequate Boolean composition operators on blobs:

- The potential field produced by the composition operator must be at least  $C^1$  continuous everywhere inside the object boundary.
- The “automatic blending” property by potential summation must be conserved through the composition.
- Blobs have bounded representation and the result of a composition must be a bounded object having its bounding box easily computed from those of the combined primitives.
- The extremities of the composition’s transition should be able to be intuitively selected once the blobs’ boundaries are fixed.

If our free-form profiles are used to combine bounded primitives, the value outside the boundaries of the resulting object will not be *zero* but  $G(0,0) = k$  ( $k \in \mathbb{R}$ ) and  $C^0$  discontinuities will be introduced on the boundary where the transition is defined. This is unsuitable, and for these reasons, we propose a different and more relevant method.

As shown with the application of super-elliptic operators [11], a solution to perform bounded operators for union and intersection is to compose the boundaries of the combined primitives without smooth transition and to use an operator that provides a  $C^1$  continuous field everywhere outside the intersection of the primitives *zero* iso-potential surfaces (see Figure 9). The difference operator can not be directly obtained with this method. This is the reason why few difference operators with smooth transition exist on blobs, and this is why we treat this operator separately. Our operators  $\widehat{g}_\cup$  and  $\widehat{g}_\cap$  are then excellent candidates to be adapted and improved for our requirements. They already conserve the combined primitives’ metrics outside the region bounded by the angles  $\theta_1$  and  $\theta_2$ , and they produce the desired transition and continuity properties. The adaptation of operators  $\widehat{g}_\cup$  and  $\widehat{g}_\cap$  to blob composition operators with smooth transitions are denoted respectively  $\widetilde{g}_\cup$  and  $\widetilde{g}_\cap$ . To allow precise and intuitive control, and to respect our constraints, the transition must be defined by control points on the  $C_0$  iso-potential surface. The first transformation is to adapt the operator’s equation to the blob formulation and to define angles  $\theta_1$  and  $\theta_2$  from the user Euclidean space  $\mathbb{E}^3$  by selecting control points  $p_1(x_1, y_1, z_1)$  and  $p_2(x_2, y_2, z_2)$  on the combined blob surfaces respectively  $f_1 = C_0$  and  $f_2 = C_0$ . Points  $p_1$  and  $p_2$  must be selected inside the intersection of the blobs’ boundaries because no transition can be defined outside these limits. Indeed, at least one of the combined primitives returns *zero*. The equation is first adapted by taking into account the following properties: Potential function  $f(p) \geq 0$  inside the object and uniformly equals *zero* outside. These give us the representation shown in Figure 10 and Equation 7 for the operator  $\widetilde{g}_\cup$  applied on two blobs defined by

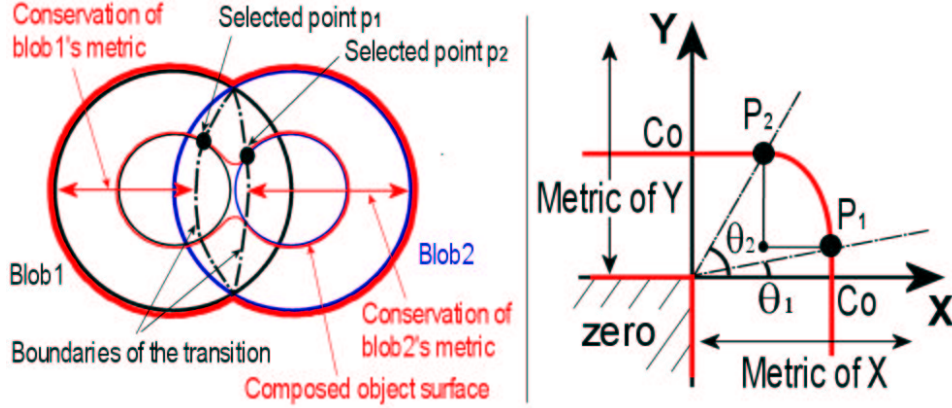


Figure 10: Union with smooth transition controlled point-by-point in the user Euclidean space  $\mathbb{E}^3$  and its function representation.

their potential functions  $f_1$  and  $f_2$  (equations of operators  $\widetilde{g}_\cap$  and  $\widetilde{g}_\cup$  are given in Appendix B).

Points  $p_1 \in \mathbb{E}^3$  and  $p_2 \in \mathbb{E}^3$  selected by the user  
correspond to points  $P_1$  and  $P_2$  such as :  
 $P_1(C_0, f_2(p_1))$  and  $P_2(f_1(p_2), C_0)$ .

$\theta_1 = \text{angle}([OX], [OP_1])$ ,  $\theta_2 = \text{angle}([OX], [OP_2])$   
At a point  $P(f_1(p), f_2(p))$  :  $\theta_P = \text{angle}([OX], [OP])$

if  $Y_P = 0$   $\widetilde{g}_\cup(X_P, Y_P) = X_P$   
if  $X_P = 0$   $\widetilde{g}_\cup(X_P, Y_P) = Y_P$   
if  $\theta_P \leq \theta_1$   $\widetilde{g}_\cup(X_P, Y_P) = X_P$   
if  $\theta_P \geq \theta_2$   $\widetilde{g}_\cup(X_P, Y_P) = Y_P$

if  $\theta_P \in ]\theta_1, \theta_2[$   $\widetilde{g}_\cup(X_P, Y_P) = C_P$   
where  $C_P$  is the solution of :

$$\frac{(X_P - C_P \cdot \cot(\theta_2))^2}{(C_P - C_P \cdot \cot(\theta_2))^2} + \frac{(Y_P - C_P \cdot \tan(\theta_1))^2}{(C_P - C_P \cdot \tan(\theta_1))^2} = 1$$

(7)

With operator  $\widetilde{g}_\cup$  in this form, only the boundaries of the transition can be controlled. For fixed angles  $\theta_1$  and  $\theta_2$  it is necessary to be able to choose the smoothness of the transition. This leads us to add at least one control point. In fact, adding one or more control points brings us to the same solution. To conserve the  $C^1$  continuity in the field, we multiply  $\widetilde{g}_\cup(P)$  by a function  $m(\theta_P)$  where  $m$  is an interpolation function of  $\mathbb{R} \rightarrow \mathbb{R}$  when  $\theta_P \in [\theta_1, \theta_2]$  and  $m(\theta_P) = 1$  otherwise. A valid graph for function  $m$  is shown in Figure 11. The link with the control points is done as follows:  $m(\theta_1) = 1, m'(\theta_1) = 0$  and  $m(\theta_2) = 1, m'(\theta_2) = 0$  to ensure  $C^1$  continuity at the beginning and the end of the transition. Then  $k_i$  ( $i > 2$ ) are computed from the control points  $p_i(x_i, y_i, z_i)$  ( $i > 2$ ) selected in the Euclidean modeling space  $\mathbb{E}^3$ . Point  $p_i$  allows us to compute the point  $P_i(f_1(p_i), f_2(p_i))$ , followed by  $\theta_{P_i}$  and  $C_i = \widetilde{g}_\cup(P_i)$ . The corresponding point  $k_i$  ( $i > 2$ ), to interpolate, has then the coordinates:  $k_i(\theta_i, C_0/C_i)$ . We have chosen one-dimensional cubic polynomial splines [32] to define function  $m$  when  $\theta_P \in [\theta_1, \theta_2]$  for their adequate smoothness and oscillation properties, and for their inexpensive computation cost. We finally obtain the union Boolean operator with

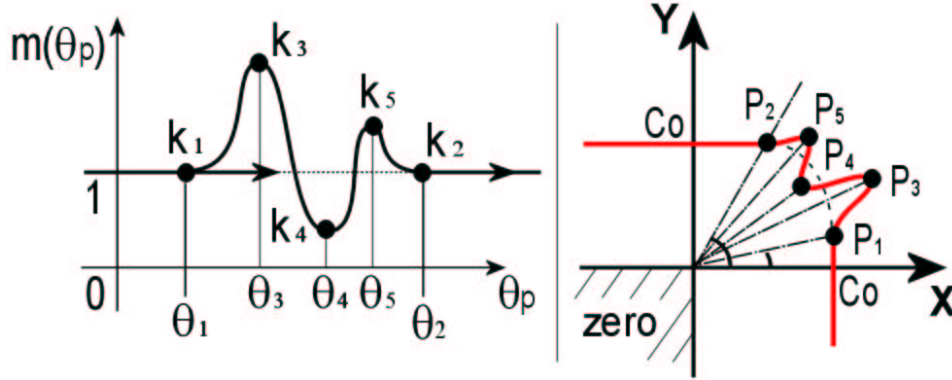


Figure 11: Graph of an interpolation function  $m(\theta_P)$  used to deform the operator  $\widetilde{g}_U$  and allow the control point-by-point of the transition.

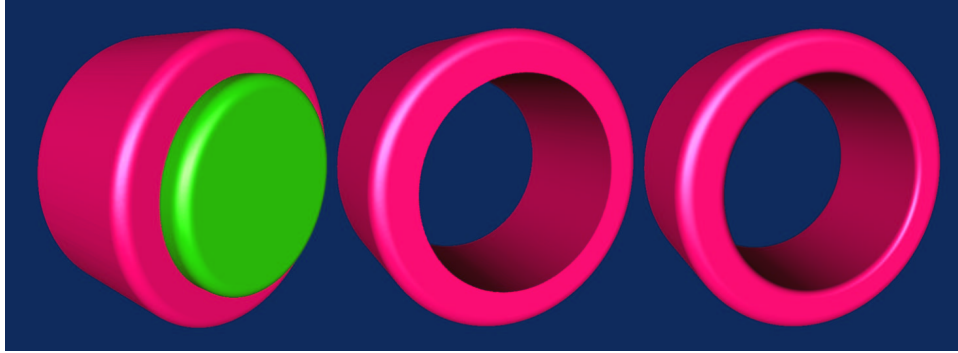


Figure 12: The ring is built using two implicit cylinders and applying subtraction, the center image uses the Ricci CSG subtraction operator, the right hand image, our smooth CSG subtraction  $\widetilde{g}_\setminus$ .

“functionally defined” transitions for blobs in Equation 8.

$$\widetilde{g}_U^{final}(P) = m(\theta_P) \cdot \widetilde{g}_U(P) \quad (8)$$

The same path has been followed to build the intersection Boolean operator with “functionally defined” transition for blobs  $\widetilde{g}_\cap^{final}(P) = m(\theta_P) \cdot \widetilde{g}_\cap(P)$  from  $\widehat{g}_\cap(P)$ .

The difference operator  $\widetilde{g}_\setminus$  cannot be obtained from operator  $\widehat{g}_\setminus$  in the same way because the  $C_0$  iso-potential surface of the blob defined by function  $f_2$  is not included in the difference of combined blob boundaries. Ricci [5] proposed the realization of the difference operator without smooth transition on blobs using the intersection operator applied on  $f_1$  and  $(2C_0 - f_2)$  instead of  $f_2$ . The same method used on our intersection operator  $\widetilde{g}_\cap^{final}$  gives the difference Boolean operator with “functionally defined” transition on blobs  $\widetilde{g}_\setminus^{final}$ . Figure 14 shows a ring object built from the ring of Figure 12 and a gem similar to that in Figure 13. The gem has been further modified by two profile curves. The first profile curve modifies the smooth intersection operation used to construct the gem. The second modifies the difference operation between the gem and a sphere (implicit point primitive) at its centre. Finally, another sphere has been added with a smooth union operation. The gem is then joined to the ring using another smooth union with a profile curve. Table 3 illustrates different union composition operators with soft transition and allows us to compare of the computation times, the potential field variations and the shape produced at the transition level. The increase of the evaluation cost of the our operators is compensated by the controllability of the form of the transition.

The bounding box of the resulting object is easy to compute. For the union operator, the box is the

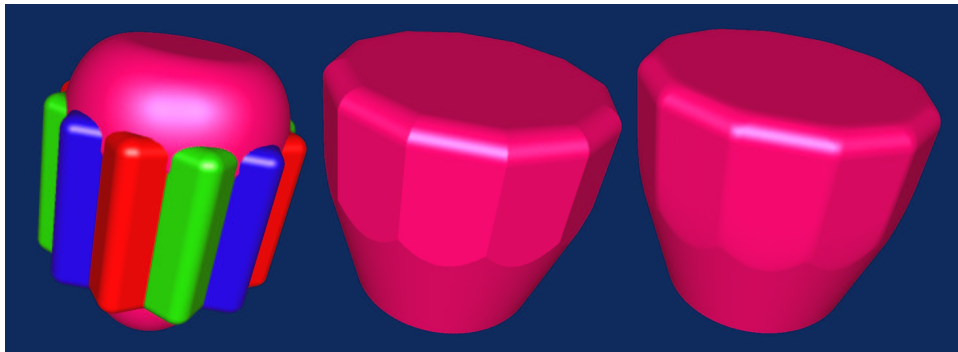


Figure 13: The gemstones are built from implicit *box* primitives and an implicit cone, center image uses the Ricci intersection operator, right hand image our smooth intersection  $\widetilde{g}_\cap$ .



Figure 14: Applying the smooth CSG operators  $\widetilde{g}_\cup$ ,  $\widetilde{g}_\cap$ ,  $\widetilde{g}_\setminus$  and profile curve operators  $\widetilde{g}_\cap^{final}$ ,  $\widetilde{g}_\setminus^{final}$  on blobs.

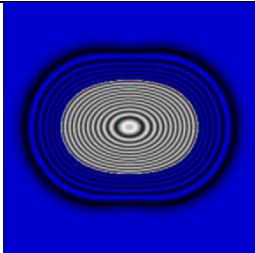
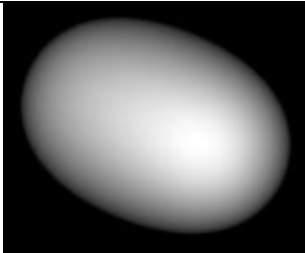
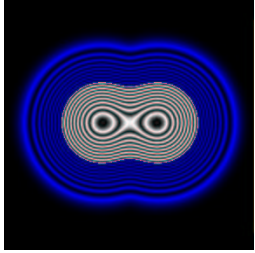
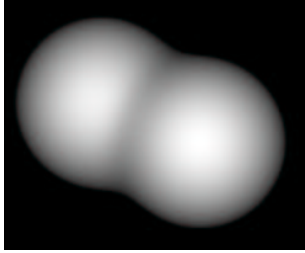
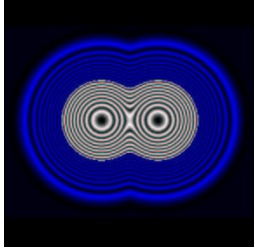
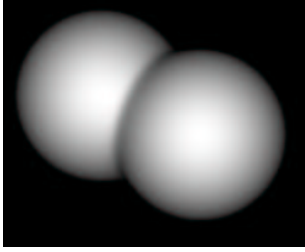
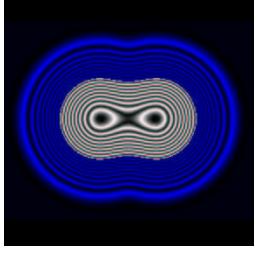
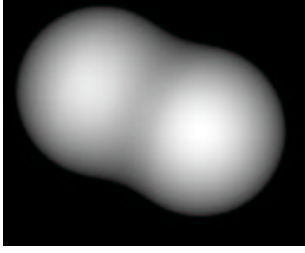
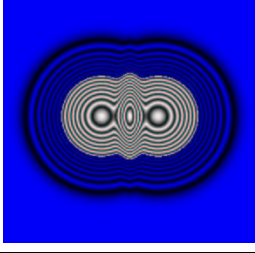
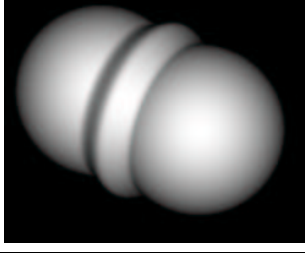
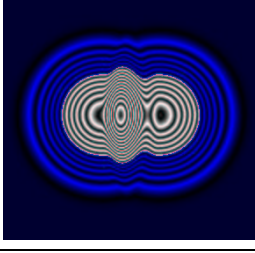
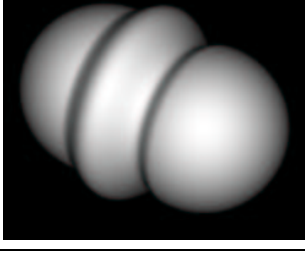
time	2D section	3D object
(a) 246		
(b) 884		
(c) 940		
(d) 1005		
(e) 1933		
(f) 2315		

Table 3: Time in milliseconds to compute potential function values for a  $128^3$  grid (2097152 evaluations). (a) Using Ricci's operator with  $n = 1$ , (b) Ricci's operator with  $n = 3$ , (c) Ricci's operator with  $n = 7$ , (d) operator  $\widetilde{g}_U$ , (e) operator  $\widetilde{g}_U^{final}$  with 3 control points and (f) operator  $\widetilde{g}_U^{final}$  with 5 control points. The middle column shows two-dimensional sections of the full grid.

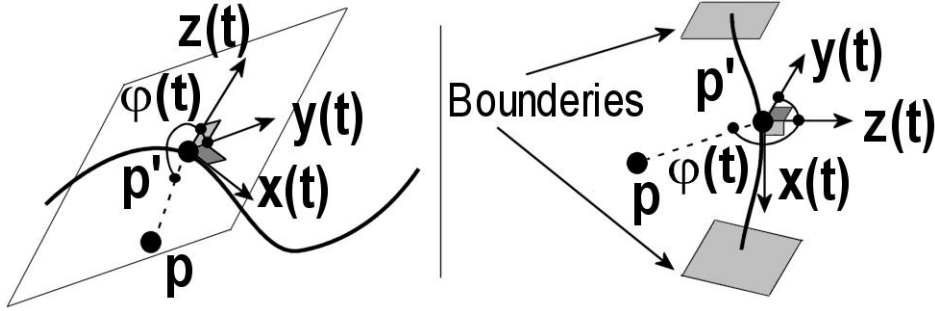


Figure 15: On the left, the trajectory and the local Cartesian coordinate system for a translational primitive. On the right, the one for a rotational primitive.

union of those of the two combined primitives. For the intersection operator, it is their intersection and for the difference it is the box of the object defined by function  $f_1$ .

A function  $m$  of  $\mathbb{R} \rightarrow \mathbb{R}$  is used to provide point-by-point control. Because such a function must be single valued, we do not obtain a true free-form control of the transition. However, blobs are bounded primitives. The transition in operators like ours is then essentially used to smooth the junction of two primitives when they are combined. We assume that in a general case, to create the desired smooth transition, three, four or five control points give enough flexibility. Free-form curves are needed in very specific cases, and often it remains easier to build a new primitive and to combine it with a smooth transition.

## 6 Sweep Objects

Sweep objects or generalized cylinders [39, 40] are well known and fully used in modeling tools based on parametric functions. Because they allow to greatly increase the variety of shapes with an intuitive formulation, implicit definitions of sweep objects have been proposed [20, 37]. Under their implicit form, these objects are based on the translational or rotational extrusion of two-dimensional implicit profiles, respectively along or around a trajectory defined by a parametric free-form curve. The parametric formulation of the trajectory allows to twist the profile or/and to interpolate several different profiles. Until now, implicit profile definition has been based on single valued function of  $R \rightarrow R$ . This consequently limits the variety of shapes that sweep objects normally provide. In this section, we explain how to use our free-form profiles to offset this restriction, and provide implicit sweep primitives  $f$  defined by the inequality  $f(p) \leq 0$ . We do not describe an entire model to define implicit sweep objects and we refer to Crespin et al [1996] and Grimm [1999] to find complete and useful models to sweep implicit profiles.

For translational primitives, profiles are defined in a local Cartesian coordinate system. To evaluate a point  $p$  of  $E^3$ , its projection  $p'$  on the trajectory is computed, and  $t$  is the value of the parameter of the curve in  $p'$ . From the parametric definition of the curve, a local Cartesian coordinate system is obtained  $(p', x(t), y(t), z(t))$ . Axis  $x(t)$  is tangent to the trajectory, and profiles are defined in the plane  $(y(t), z(t))$  (see Figure 15). Our profile is then defined as  $G(y(t), z(t))$ . For bounded trajectories, the extremities can be closed by computing the profile coordinates as  $G(\rho(t).cos(\varphi(t)), \rho(t).sin(\varphi(t)))$  where  $\rho(t)$  is the distance between the evaluated point  $p$  of  $E^3$  and its projection  $p'$ , and  $\varphi(t)$  is the angle between  $p$  and  $y(t)$ . Profiles are not directly defined as  $G(\rho(t), \varphi(t))$  because  $\varphi(t)$  varies in  $[\alpha, \alpha + \pi/2[$ , and a  $C^0$  discontinuity is generated at  $\varphi(t) = \alpha$  in the potential field defined by  $G$ .

For rotational primitives, the same cartesian coordinate system is computed. Profiles are defined along the trajectory for fixed values of  $\varphi(t)$ , and extruded around it. The profile is then defined as  $G(\rho, t)$  where  $\rho$  is the distance between the point  $p$  and its projection  $p'$ , and  $t$  is the parameter value of the trajectory at point  $p'$ . If the trajectory is bounded, a particular attention has to be focussed on the extremities of the trajectories. Indeed, as illustrated in Figure 15 the profile must be defined in the boundaries fixed by the limits of variation of the parameter along the profile.

Figure 16 shows an example of translational primitive. Three profiles are defined along the trajectory

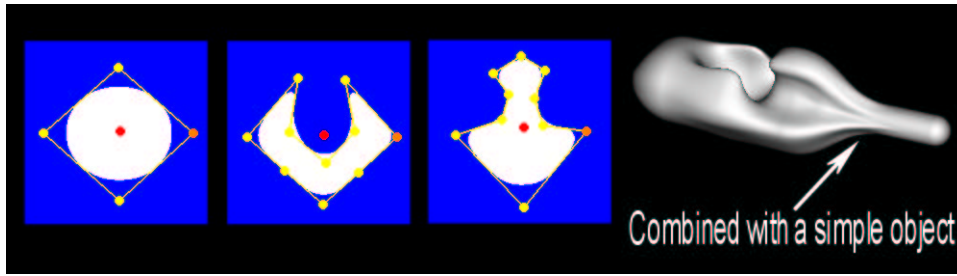


Figure 16: **Example of implicit sweep object.** The three shown profiles are extruded along a line segment, and the resulting object is combined with a simple primitive using our composition method (see Section 4).

and interpolated with cubic functions. One can notice that the trajectory is outside the second profile. Because our profiles provide regular and homogenous field variations, our sweep objects can be correctly combined with other volume objects.

## 7 Conclusion and Future Work

Accurate and intuitive manipulation of volume objects is the next required step to provide efficient volume modelling software. In this paper we have presented some solutions to these requirements when volumes are composed. Recent work introduced the notion of “implicit spaces” as a theoretical base to accurately control the transitions [18] and we have shown how this leads us to the study of free-form implicit curves controlled point-by-point. Profiles require regular variations of their two-dimensional potential field and the control of their extremities. The adaptation of a method proposed by Pasko et al [36] has allowed us to provide open and closed profiles, defining line segments or smooth curves, with sufficient properties.

To manipulate volumes defined by the inequality  $f(p) \leq 0$ , we have grouped in a single modeling tool: creation, sculpture and Boolean composition operators with sharp or smooth free-form transitions. We have shown how accuracy is ensured and explained how to understand and use our modeling metaphor in an efficient way. The techniques described in this paper generalize the models given in [18] and provide controllability and freedom of expression to the user and greatly extend the possibilities offered by operators on volumetric objects. The point-by-point control curve provides the possibility of interactively designing blended shapes, however more work needs to be done on volume data structure manipulation and modeling interface design to add interactivity to the modeling process. Adaptive structures like ADF [3] and interactive ray casting algorithm for isosurface visualization [1] can be used respectively to store a sampled potential field and accurately render the surface. A sampled field structure stores the potential values after each operation, removing the expensive evaluation of an increasingly complicated potential field function. This technique allows us to accurately render the modeled object directly without the use of an additional data structure like polygons. These reasons provide a good justification for the investigation of the combination of these techniques, to provide interactive volume modeling solutions.

Because sampled volumes are large data structures, the development of multiresolution techniques to store and reconstruct potential fields represents another important step.

Free-form profiles can also be used in implicit sweep objects [20, 37]. Indeed, only profiles defined by single valued functions of  $\mathbb{R} \rightarrow \mathbb{R}$  are used in implicit modeling, while there is no apparent reason to limit the user by the form of the profile they want to sweep. Our profiles allowed us to create swept objects defined by an inequality  $f(p) \leq 0$ . Since they have regular and homogenous field variations, sweep objects are correctly combined with other volume objects.

## 8 Acknowledgments

This work was partially funded by E.U. contract HPRN-CT-1999-00117

## References

- [1] M. Chen, A. Kaufman and R. Yagel. *Volume Graphics*, Springer, London, 2000.
- [2] K. Engel, M. Krauss and T. Ertl. High-quality Preintegrated Volume rendering Using Hardware-accelerated Pixel Shading. *Proc. of EUROGRAPHICS/SIGGRAPH Graphics Hardware Workshop*, 2001.
- [3] S.F. Frisken, R.N. Perry, A.P. Rockwood and T.R. Jones. Adaptatively Sampled Distance Fields: A General representation of Shape for Computer Graphics. *Proceedings of SIGGRAPH 2000*, Computer Graphics Proceedings, Annual Conference Series, pp. 249–254, 2000.
- [4] L.P. Kobbelt, M. Botsch, U. Schwanecke and H.P. Seidel. Feature Sensitive surface Extraction from Volume data. *Proceedings of SIGGRAPH 2001*, Computer Graphics Proceedings, Annual Conference Series, pp. 57–66, 2001.
- [5] A. Ricci. A Constructive Geometry for Computer Graphics. *The Computer Journal*, **16** (2), pp. 157–160, 1973.
- [6] J. F. Blinn. A Generalization of algebraic surface drawing. *ACM Transaction on Graphics*, **1** (3), pp. 235–256, 1982.
- [7] J. Bloomenthal and B. Wyvill. Interactive techniques for Implicit Modeling. *Computer Graphics (Proc. of SIGGRAPH 1990)*, **24** (2), pp. 109–116, 1990.
- [8] A. P. Rockwood. The Displacement Method for Implicit Blending Surfaces in Solid Models. *ACM Transaction on Graphics*, **8** (4), pp. 279–297, 1989.
- [9] A. Sourin and A. Pasko. Function Representation for Sweeping by a Moving Solid. *IEEE Transaction on Visualization and Computer Graphics*, **2** (1), pp. 11–18, 1996.
- [10] A. Pasko, V. Adzhiev, A. Sourin and V. Savchenko. Function Representation in Geometric Modeling: concepts, Implementation and Applications. *The Visual Computer*, **8** (2), pp. 429–446, 1995.
- [11] B. Wyvill and A. Guy and E. Galin. Extending the CSG Tree: Warping, Blending and Boolean Operations in an Implicit Surface Modeling System. *Computer Graphics Forum*, **18** (2), pp. 149–158, 1999.
- [12] M. Chen and J. Tucker. Constructive Volume Geometry. *Computer Graphics Forum*, **19** (4), pp. 281–293, 2000.
- [13] H. Nishimura, M. Hirai, T. Kawai, I. Shirakara and K. Omura. Object Modeling by Distribution Functions. *Electronics Communications (in Japanese)*, **J68** (D), pp. 718–725, 1985.
- [14] G. Wyvill, C. McPheeters and B. Wyvill. Data Structure for Soft Objects. *The Visual Computer*, **2** (4), pp. 227–234, 1986.
- [15] C. Galbraith, P. Prusinkiewicz and B. Wyvill. Modeling Murex Cabritii Sea Shell with a Structured Implicit Modeler. *Proc. of Computer Graphics International 2000*, 2000.
- [16] C. Hoffmann and J. Hopcroft. Automatic Surface Generation in Computer Aided Design. *The Visual Computer*, **1**, pp. 92–100, 1985.
- [17] V. Adzhiev, M. Kazakov and A. Pasko. Hybrid System Architecture for Volume Modeling. *Computer and Graphics*, **24** (1), pp. 67–78, 2000.
- [18] L. Barthe, V. Gaildrat and R. Caubet. Extrusion of 1D implicit profiles: Theory and first application. *International Journal of Shape Modeling*, **7** (2), pp. 179–199, 2001.
- [19] L. Barthe, B. Mora, N. Dodgson and M. Sabin. Triquadratic reconstruction for interactive modelling of potential fields. *Proc. of Shape Modeling International 2002*, pp. 145–153, 2002.

- [20] B. Crespin, C. Blanc and C. Schlick. Implicit Sweep Objects. *EUROGRAPHICS 1996*, **15** (3), pp. 165–174, 1996.
- [21] Z. Kacic-Alesic and B. Wyvill. Controlled Blending of Procedural Implicit Surfaces. *Proc. of Graphic Interface 1991*, pp. 236–245, 1991.
- [22] Ca. Blanc and C. Schlick. Extended Field Functions for Soft Objects. *Proc. of Implicit Surfaces 1995*, pp. 21–32, 1995.
- [23] M. Desbrun and M.P. Gascuel. Animating Soft Substances with Implicit Surfaces. *Computer Graphics (Proc. of SIGGRAPH 1995)*, pp. 287–290, 1995.
- [24] A. Guy and B. Wyvill. Controlled Blending for Implicit Surfaces Using a Graph. *Proc. of Implicit Surfaces 1995*, pp. 107–112, 1995.
- [25] E. Ferley and M. P. Cani and J. D. Gascuel. Practical Volumetric Sculpting. *The Visual Computer*, **16** (8), pp. 469–480, 2000.
- [26] E. Galin and S. Akkouche. Incremental Polygonization of Implicit Surfaces. *Graphical Models*, **62** (1), pp. 19–39, 2000.
- [27] B.A. Payne and A.W. Toga. Distance Field Manipulation of Surface Models. *Computer Graphics and Applications*, **12** (1), pp. 65–71, 1992.
- [28] M. Jones and R. Satherley. Shape Representation Using Space Filled Sub-voxel Distance Fields. *Proc. of Shape Modeling International 2001*, pp. 316–325, 2001.
- [29] J.C. Carr, R.K. Beaton, J.B. Cherrie, T.J. Mitchell, W.R. Fright, B.C. McCallum and T.R. Evans. Reconstruction and Representation of 3D Objects with Radial Basis Functions. *Proceedings of SIGGRAPH 2001*, Computer Graphics Proceedings, Annual Conference Series, pp. 67–76, 2001.
- [30] A. E. Middleditch and K. H. Sears. Blend Surfaces for Set-theoretic Volume Modelling Systems. *Computer Graphics*, **19** (3), pp. 161–170, 1985.
- [31] D. Dekkers, K. van Overveld and R. Golsteijn. Combining CSG Modeling with Soft Blending using Lipschitz-based Implicit Surfaces. *Technical Report, Eindhoven University of Technology, Computer Graphics Group*, 1997.
- [32] I.D. Faux and M.J. Pratt. *Computational Geometry for Design and Manufacture*, Ellis Horwood, 1979.
- [33] R.N. Goldman, T.W. Sederberg and D.C. Anderson. Vector Elimination: A Technique for the Implicitization, Inversion, and Intersection of Planar Parametric Rational Polynomial Curves. *Computer Aided Geometric Design*, **1** (4), pp. 327–356, 1984.
- [34] C.M. Hoffmann. Implicit Curves and Surfaces in CAGD. *IEEE Computer Graphics and Applications*, **13** (1), pp. 79–88, 1993.
- [35] K.T. Miura, A.A. Pasko and V.V. Savchenko. Parametric Patches and Volumes in Function Representation of Geometric Solids. *Proc. of CSG 1996*, pp. 217–231, 1996.
- [36] A.A. Pasko, A.V. Savchenko and V.V. Savchenko. Implicit Curved Polygons. *Technical Report 96-1-004, University of Aizu, Japan*, 1996.
- [37] C. Grimm. Implicit Generalized Cylinders Using Profile Curves. *Proc. of Implicit Surfaces 1999*, pp. 33–41, 1999.
- [38] B. Mora, J.P. Jessel and R. Caubet. Visualizaton of Isosurfaces with Parametric Cubes. *EUROGRAPHICS 2001 Proc.*, **20** (3), pp. 377–384, 2001.

- [39] S. Coquillard. A Control Point Based Sweeping technique. *IEEE Computer Graphics and Applications*, **7** (11), pp. 36–44, 1987.
- [40] W. Bronswoort, P. van Nieuwenhuizen and F. Post. Display of Profiled Sweep Objects. *The Visual Computer*, **5**, pp. 147–157, 1989.

## A Operators $\widehat{g}_\cap$ and $\widehat{g}_\setminus$

- Operator  $\widehat{g}_\cap$ :

$$\theta_1 \in ]0, \pi/4[, \quad \theta_2 \in ]\pi/4, \pi/2[.$$

$$\text{At a point } P(X_P, Y_P) : \quad \theta_P = \text{angle}([OX], [OP])$$

$$\text{if } X_P = Y_P = 0 \quad \widehat{g}_\cap(X_P, Y_P) = 0$$

$$\text{if } \theta_P \in [\theta_2 - \pi, \theta_1] \quad \widehat{g}_\cap(X_P, Y_P) = X_P$$

$$\text{if } \theta_P \in [\theta_2, \theta_1 + \pi] \quad \widehat{g}_\cap(X_P, Y_P) = Y_P$$

$$\text{if } \theta_P \in ]\theta_1, \theta_2[ \quad \widehat{g}_\cap(X_P, Y_P) = C_P$$

where  $C_P$  is the solution of :

$$\frac{(X_P - C_P \cdot \cot(\theta_2))^2}{(C_P - C_P \cdot \cot(\theta_2))^2} + \frac{(Y_P - C_P \cdot \tan(\theta_1))^2}{(C_P - C_P \cdot \tan(\theta_1))^2} = 1$$

$$\text{if } \theta_P \in ]\theta_1 + \pi, \theta_2 + \pi[ \quad \widehat{g}_\cap(X_P, Y_P) = C_P$$

where  $C_P$  is the solution of :

$$\frac{(C_P \cdot \cot(\theta_1) - X_P)^2}{(C_P \cdot \cot(\theta_1) - C_P)^2} + \frac{(C_P \cdot \tan(\theta_2) - Y_P)^2}{(C_P \cdot \tan(\theta_2) - C_P)^2} = 1$$

- Operator  $\widehat{g}_\setminus$ :

Operator  $\widehat{g}_\setminus$  is directly obtained from operator  $\widehat{g}_\cap$  using the following expression:

$$\widehat{g}_\setminus(X, Y) = \widehat{g}_\cap(X, -Y)$$

## B Operators $\widetilde{g}_\cap$ and $\widetilde{g}_\setminus$

- Operator  $\widetilde{g}_\cap$ :

To points  $p_1 \in \mathbb{E}^3$  and  $p_2 \in \mathbb{E}^3$  selected by the user correspond points  $P_1$  and  $P_2$  such as :

$$P_1(C_0, f_2(p_1)) \quad \text{and} \quad P_2(f_1(p_2), C_0).$$

$$\theta_1 = \text{angle}([OX], [OP_1]), \quad \theta_2 = \text{angle}([OX], [OP_2])$$

$$\text{At a point } P(f_1(p), f_2(p)) : \quad \theta_P = \text{angle}([OX], [OP])$$

$$\text{if } Y_P = 0 \quad \widetilde{g}_\cap(X_P, Y_P) = 0$$

$$\text{if } X_P = 0 \quad \widetilde{g}_\cap(X_P, Y_P) = 0$$

$$\text{if } \theta_P \leq \theta_1 \quad \widetilde{g}_\cap(X_P, Y_P) = Y_P$$

$$\text{if } \theta_P \geq \theta_2 \quad \widetilde{g}_\cup(X_P, Y_P) = X_P$$

$$\text{if } \theta_P \in ]\theta_1, \theta_2[ \quad \widetilde{g}_\cup(X_P, Y_P) = C_P$$

where  $C_P$  is the solution of :

$$\frac{(C_P \cdot \cot(\theta_1) - X_P)^2}{(C_P \cdot \cot(\theta_1) - C_P)^2} + \frac{(C_P \cdot \tan(\theta_2) - Y_P)^2}{(C_P \cdot \tan(\theta_2) - C_P)^2} = 1$$

- Operator  $\widetilde{g}_\setminus$ :

Operator  $\widetilde{g}_\setminus$  is directly obtained from operator  $\widetilde{g}_\cap$  using the following expression:

$$\widetilde{g}_\setminus(X, Y) = \widetilde{g}_\cap(X, 2 \cdot C_0 - Y)$$

## C Closed form solution for the evaluation of $C_P$ in our new composition operators

- Solution for the equation:

$$\frac{(C_P \cdot \cot(\theta_1) - X_P)^2}{(C_P \cdot \cot(\theta_1) - C_P)^2} + \frac{(C_P \cdot \tan(\theta_2) - Y_P)^2}{(C_P \cdot \tan(\theta_2) - C_P)^2} = 1$$

$C_P$  is the greater solution of the following equation:

$$a \cdot C_P^2 + b \cdot C_P + c = 0$$

with

$$\begin{aligned} a &= \frac{(\tan(\theta_2) - 1)^2}{\tan^2(\theta_1)} + \tan^2(\theta_2) \cdot \left( \frac{1}{\tan(\theta_1)} - 1 \right)^2 \\ &\quad - \left( \frac{1}{\tan(\theta_1)} - 1 \right)^2 \cdot (\tan(\theta_2) - 1)^2 \\ b &= -2 \cdot \left( X_P \cdot \frac{(\tan(\theta_2) - 1)^2}{\tan(\theta_1)} + Y_P \cdot \tan(\theta_2) \cdot \left( \frac{1}{\tan(\theta_1)} - 1 \right)^2 \right) \\ c &= X_P^2 \cdot (\tan(\theta_2) - 1)^2 + Y_P^2 \cdot \left( \frac{1}{\tan(\theta_1)} - 1 \right)^2 \end{aligned}$$

$C_P$  is then obtained with:

$$C_P = \frac{-b + \sqrt{(b^2 - 4 \cdot a \cdot c)}}{2 \cdot a}$$

- Solution for the equation:

$$\frac{(X_P - C_P \cdot \cot(\theta_2))^2}{(C_P - C_P \cdot \cot(\theta_2))^2} + \frac{(Y_P - C_P \cdot \tan(\theta_1))^2}{(C_P - C_P \cdot \tan(\theta_1))^2} = 1$$

$C_P$  is the lower solution of the following equation:

$$a.C_P^2 + b.C_P + c = 0$$

with

$$a = \frac{(\tan(\theta_1) - 1)^2}{\tan^2(\theta_2)} + \tan^2(\theta_1) \cdot \left( \frac{1}{\tan(\theta_2)} - 1 \right)^2 - \left( \frac{1}{\tan(\theta_2)} - 1 \right)^2 \cdot (\tan(\theta_1) - 1)^2$$

$$b = -2 \cdot \left( X_P \cdot \frac{(\tan(\theta_1) - 1)^2}{\tan(\theta_2)} + Y_P \cdot \tan(\theta_1) \cdot \left( \frac{1}{\tan(\theta_2)} - 1 \right)^2 \right)$$

$$c = X_P^2 \cdot (\tan(\theta_1) - 1)^2 + Y_P^2 \cdot \left( \frac{1}{\tan(\theta_2)} - 1 \right)^2$$

$C_P$  is then obtained with:

$$C_P = \frac{-b - \sqrt{(b^2 - 4.a.c)}}{2.a}$$

- All the terms in  $\theta_1$  and  $\theta_2$  can be precomputed (once  $\theta_1$  and  $\theta_2$  are selected), which greatly decreases the cost of the evaluation of  $C_P$ . For instance,  $a$  can be totally pre-computed.